

Comparison of the Solution Nuclear Magnetic Resonance and Crystal Structures of Interleukin-8

Possible Implications for the Mechanism of Receptor Binding

G. Marius Clore and Angela M. Gronenborn

Laboratory of Chemical Physics, Building 2, Room 123
National Institute of Diabetes and Digestive and Kidney Diseases
National Institutes of Health, Bethesda, MD 20892, U.S.A.

(Received 24 August 1990; accepted 12 October 1990)

A comparison of the solution structure of the interleukin-8 dimer determined by nuclear magnetic resonance spectroscopy with that of the 2 Å resolution X-ray structure, solved by molecular replacement using the solution structure as a starting model, is presented. At the monomer level the atomic root-mean-square difference between the two structures for residues 7 to 72 is ~ 1.1 Å for the backbone atoms, ~ 1.6 Å for all atoms, and ~ 1 Å for all atoms of the internal residues. There are two main regions of difference in the monomer. In the X-ray structure residues 4 to 6 are well ordered and the charged groups of Glu4 of one subunit and Lys23' of the other are in close enough proximity to form an electrostatic interaction. In contrast, these residues are partially disordered in solution and the electrostatic interaction involving Glu4 is replaced by one between Glu29 of one subunit and Lys23' of the other. In the loop comprising residues 31 to 36, His33 accepts a hydrogen bond from the backbone amide group of Gln8 in the solution structure, but donates a hydrogen bond to the backbone carbonyl group of Glu29 in the X-ray structure. There is also a difference in the quaternary structure with regard to the relative orientation of the two subunits produced by a rigid body rotation about the C_2 axis that alters the angle between the central β -strands (formed by residues 23 to 29 of the 2 subunits) at the dimer interface, without breaking the symmetry. In the solution structure this angle has a value of 168° , while in the X-ray structure the central strands are essentially flat, with an angle of 179° . As a result, the separation between the two anti-parallel helices, which lie at an angle of about 60° to the underlying β -strands, is decreased from 14.8 Å in the solution structure to 11.1 Å in the X-ray structure. The quaternary structural difference is related to the different conformations of the N terminus and the 31 to 36 loop, both of which display different interactions with respect to the ends of the central β -strands in the two structures. These findings indicate that interleukin-8 has the potential to undergo conformational transitions that may be of functional significance.

Interleukin-8 (IL-8 \dagger) is a member of the cytokine family of proteins that play a key role in the immune and inflammatory responses (for a review, see Matsushima & Oppenheim, 1989). It is a small dimeric protein (Clore *et al.*, 1989), composed of two identical subunits (each ~ 8000 Da), that is released from several cell types and exhibits two major activities. The first is the specific promotion of

neutrophil, basophil and T-cell chemotaxis, and the second involves neutrophil activation. Sequence comparisons have revealed that IL-8 belongs to a large superfamily of proteins involved in the immune and inflammatory responses and in the mediation of cell growth (Matsushima & Oppenheim, 1989; Leonard & Yoshimura, 1990).

Recently, we presented the determination of a high-resolution structure of IL-8 in solution by nuclear magnetic resonance (n.m.r.: Clore *et al.*, 1990). Subsequently, the X-ray structure of IL-8 was solved by necessity using the n.m.r. structure as a starting model for molecular replacement, as other methods proved to be unsuccessful (Baldwin *et al.*, 1990). In particular, no suitable heavy-atom derivatives for isomorphous replacement could be

\dagger Abbreviations used: IL-8, interleukin-8; PF4, platelet factor-4; n.m.r., nuclear magnetic resonance; SA, simulated annealing; r.m.s., root mean square; NOE, nuclear Overhauser enhancement; p.p.m., parts per million; GRO, growth related gene product; MIP, macrophage inflammatory protein.

Table 1
Comparison of structural statistics for the n.m.r. and X-ray structures of IL-8 and atomic r.m.s. differences between the structures

A. Structural statistics

	n.m.r. <SA>	X-ray
r.m.s. deviations from expt n.m.r.		
distance restraints (Å)†		
all (1880)	0.031 ± 0.002 (0)	0.181 (34,18)
Intrasubunit		
Interresidue short range ($ i-j \leq 5$) (784)	0.019 ± 0.002 (0)	0.156 (10,8)
Interresidue long range ($ i-j > 5$) (370)	0.027 ± 0.003 (0)	0.215 (6,6)
Intraresidue (540)	0.044 ± 0.002 (0)	0.116 (10,0)
H-bond (104)‡	0.031 ± 0.003 (0)	0.392 (4,4)
Intersubunit		
Interproton (70)	0.022 ± 0.008 (0)	0.189 (4,0)
H-bond (12)‡	0.004 ± 0.006 (0)	0.000 (0)
r.m.s. deviations from expt n.m.r. dihedral restraints (deg.) (362)§	0.203 ± 0.040 (0)	18.7 (20)

B. Atomic r.m.s. differences for the monomer

	Atomic r.m.s. differences (Å)				
	Backbone atoms		All atoms		
	7-72	7-30, 34 and 37-72	7-72	7-30, 34 and 37-72	Internal residues
A. n.m.r. versus X-ray					
<SA> versus X-ray	1.14 ± 0.09	0.89 ± 0.071	1.82 ± 0.08	1.66 ± 0.07	1.12 ± 0.07
\overline{SA} versus X-ray	1.10	0.84	1.64	1.45	1.00
$(\overline{SA})_r$ versus X-ray	1.11	0.84	1.71	1.53	1.02
B. n.m.r.					
<SA> versus \overline{SA}	0.30 ± 0.06	0.29 ± 0.06	0.80 ± 0.05	0.82 ± 0.05	0.51 ± 0.05
<SA> versus $(\overline{SA})_r$	0.34 ± 0.06	0.33 ± 0.05	0.91 ± 0.06	0.92 ± 0.06	0.59 ± 0.06
$(\overline{SA})_r$ versus \overline{SA}	0.16	0.16	0.42	0.43	0.30

The notation of the structures is as follows: <SA> are the final 30 dynamical simulated annealing structures derived from the solution n.m.r. data for IL-8; \overline{SA} is the mean structure obtained by averaging the co-ordinates of the individual SA dimer structures (excluding residues 1 to 5 of both subunits); $(\overline{SA})_r$ is the restrained minimized mean structure obtained by restrained minimization of \overline{SA} ; X-ray is the X-ray structure of IL-8. The number of terms for the various restraints are given in parentheses.

† The numbers in parentheses following the r.m.s. deviations indicate the number of NOE violations; the 1st number gives the violations between 0.5 to 1.0 Å, the 2nd number the violations between 1.0 to 2.0 Å. In the case of the n.m.r. structures there are no violations greater than 0.5 Å.

‡ For each backbone hydrogen bond there are 2 restraints: r_{NH-O} , 1.7 to 2.3 Å; r_{N-O} , 2.4 to 3.3 Å. Although these were identified on the basis of a qualitative interpretation of the NOE and NH exchange data, they were included only as restraints in the simulated annealing calculations after they could be unambiguously assigned following the initial structure calculations (Clore *et al.*, 1990).

§ The torsion angle restraints comprise 136 ϕ , 122 ψ and 104 χ_1 angles per dimer. The numbers in parentheses following the r.m.s. deviations are the number of angles that deviate by more than 10 degrees from the upper and lower bounds of the restraints.

|| The internal residues, defined by an accessible surface area of ≤ 100 Å², comprise residues 7, 9, 12 to 14, 16 to 19, 21, 22, 24, 25, 27, 28, 30, 34, 37 to 41, 43, 45, 46, 49 to 53, 57 to 59, 61, 62, 65, 66 and 69.

obtained despite several years of trying (A. Wlodawer, personal communication). In this communication, we present a comparison of the n.m.r. and X-ray structures that reveals a number of genuine structural differences between the solution and crystal states.

The solution n.m.r. structure was determined on the basis of 1880 experimental distance restraints (of which 82 are intersubunit) and 362 torsion angle restraints (comprising ϕ , ψ and χ_1 torsion angles) (Clore *et al.*, 1990). A total of 30 simulated annealing (SA) structures was obtained and the atomic root-

mean-square (r.m.s.) distribution (excluding residues 1 to 5 of each subunit) of the individual dimeric SA structures about the mean co-ordinate positions was 0.41 Å (1 Å = 0.1 nm) for the backbone atoms and 0.9 Å for all atoms (Clore *et al.*, 1990). The X-ray structure at 2 Å resolution was solved by molecular replacement using the restrained minimized mean n.m.r. structure as a starting model and subsequently refined to an *R*-factor of 18.7% with good covalent geometry (Baldwin *et al.*, 1990). With the exception of residues 1 to 3, which could not be located, all residues were well placed in electron

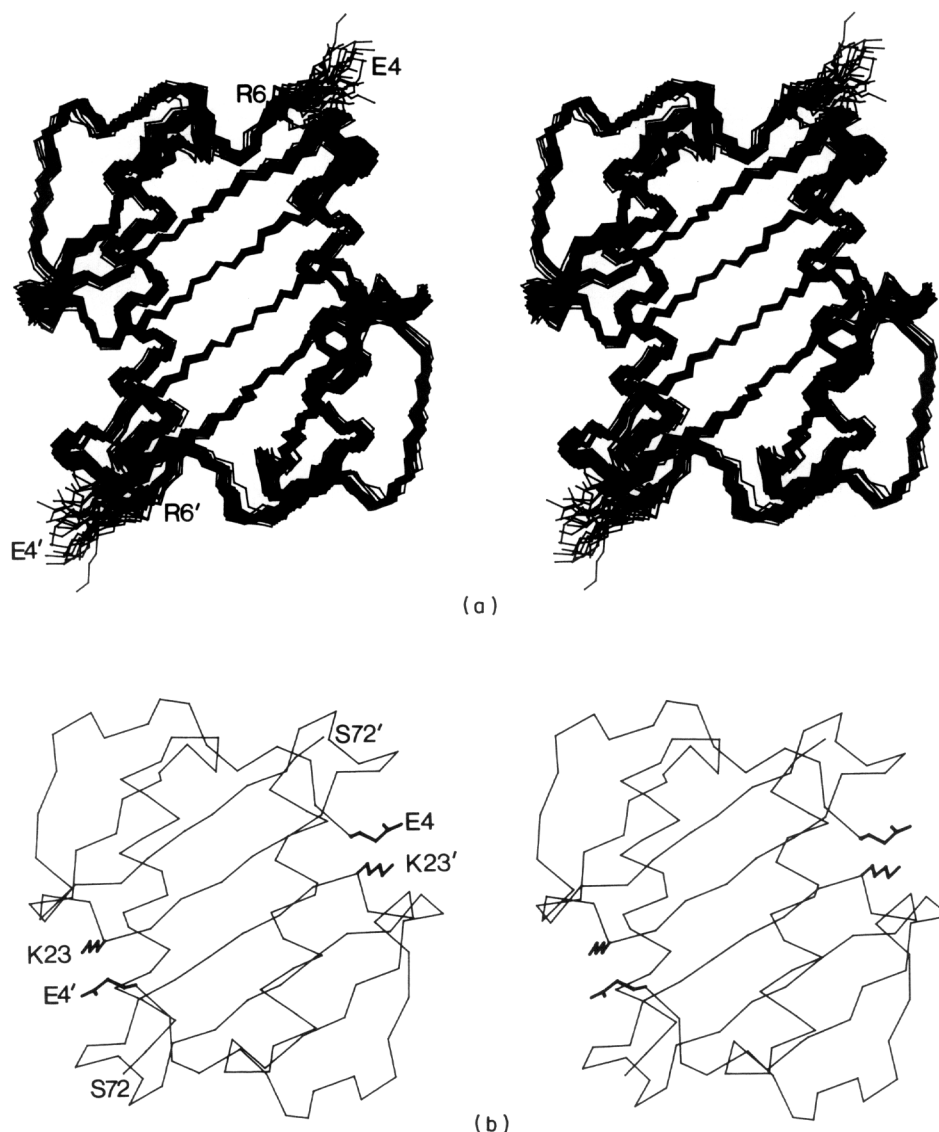


Figure 1. (a) Stereoview of the backbone (N, C α , C) atoms of the 30 SA n.m.r. structures of IL-8; (b) stereoview of the C α atoms of the X-ray structure of IL-8 together with the side-chains for Glu4 and Lys23. Note the electrostatic interaction between Glu4 of one subunit and Lys23' of the other in the X-ray structure, which is not present in the n.m.r. structures. Although the N terminus is disordered in the n.m.r. structure, it is readily seen that in no case do residues 4 and 5 in the SA n.m.r. structures overlap with residues 4 to 5 of the X-ray structure.

density, with no breaks in the main-chain regions. A summary of the agreement with the experimental n.m.r. restraints for the X-ray and n.m.r. structures and of the atomic r.m.s. differences between the structures is given in Table 1.

The overall molecular architecture and backbone hydrogen bonding of the n.m.r. and X-ray structures are essentially identical (Fig. 1), and the quaternary structure of IL-8 is a dimer both in solution and in the crystal. Although there was a question mark regarding the monomeric *versus* dimeric nature of the protein in earlier work (Yoshimura *et al.*, 1987), the n.m.r. results indicate conclusively that IL-8 is a dimer in solution that remains stably associated at pH 6.5 over a concentration range, 0.3 to 15 mg/ml, as evidenced by the absence of any changes in either chemical shifts or linewidths (our unpublished data).

As residues 1 to 3 are completely disordered and residues 4 to 6 partially disordered in solution, as evidenced by the absence of any NOEs for the first two residues and the presence of only sequential C α H(*i*)-NH(*i*+1) NOEs for residues 3 to 6 (Clare *et al.*, 1990), the quantitative comparison of the two structures was restricted to residues 7 to 72. Stereoviews providing a comparison of the backbone and selected side-chains of the n.m.r. and X-ray structures are afforded in Figures 1 and 2 and Figures 3 and 4, respectively.

The backbone (N, C α , C, O) atomic r.m.s. difference between the monomer units of the X-ray and the restrained minimized mean n.m.r. structures is 1.1 Å for residues 7 to 72. The backbone atomic r.m.s. difference between the two structures for the dimer is significantly larger (~ 2 Å), and, as will be discussed below, is due to a difference in the relative

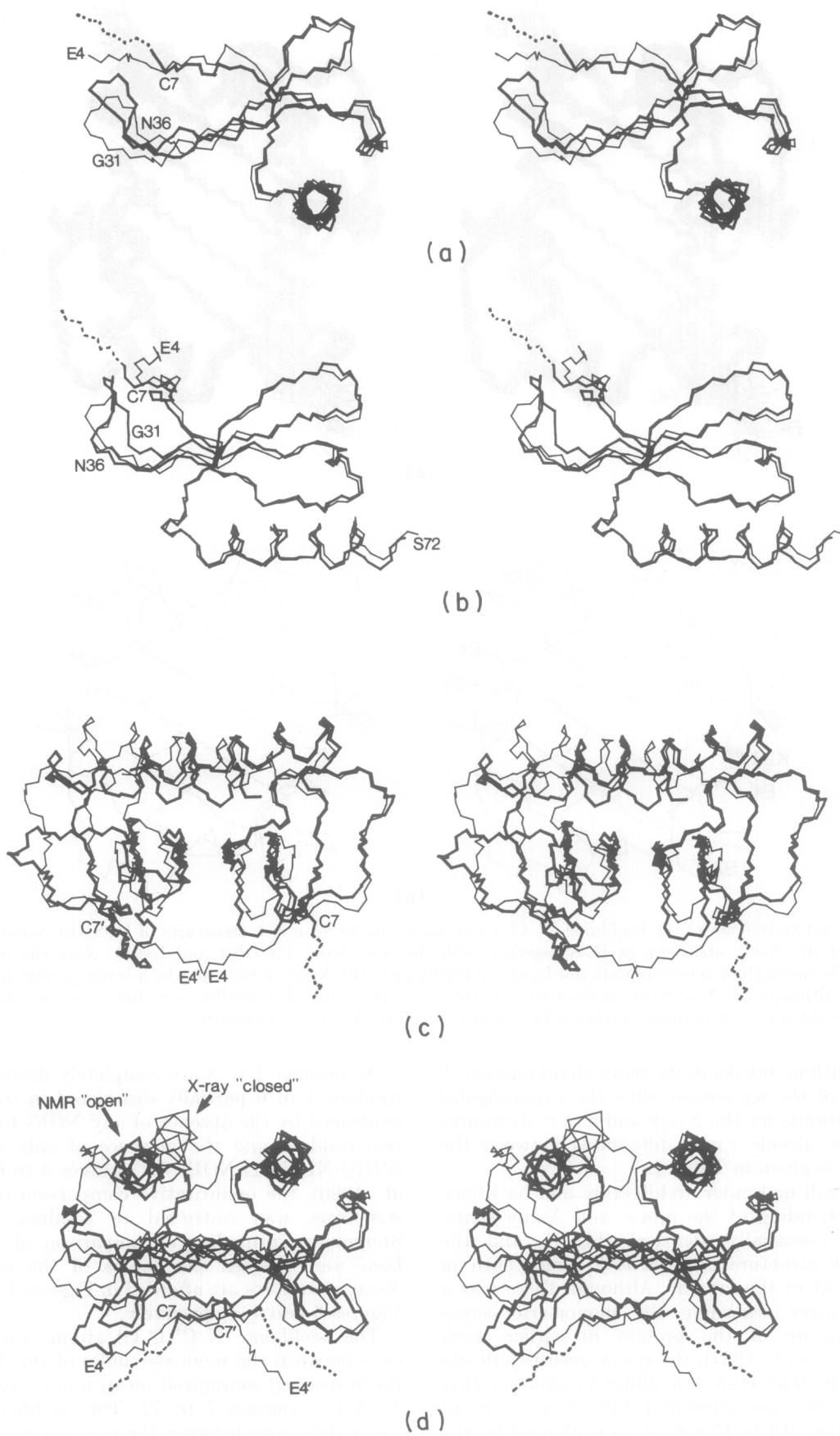


Fig. 2.

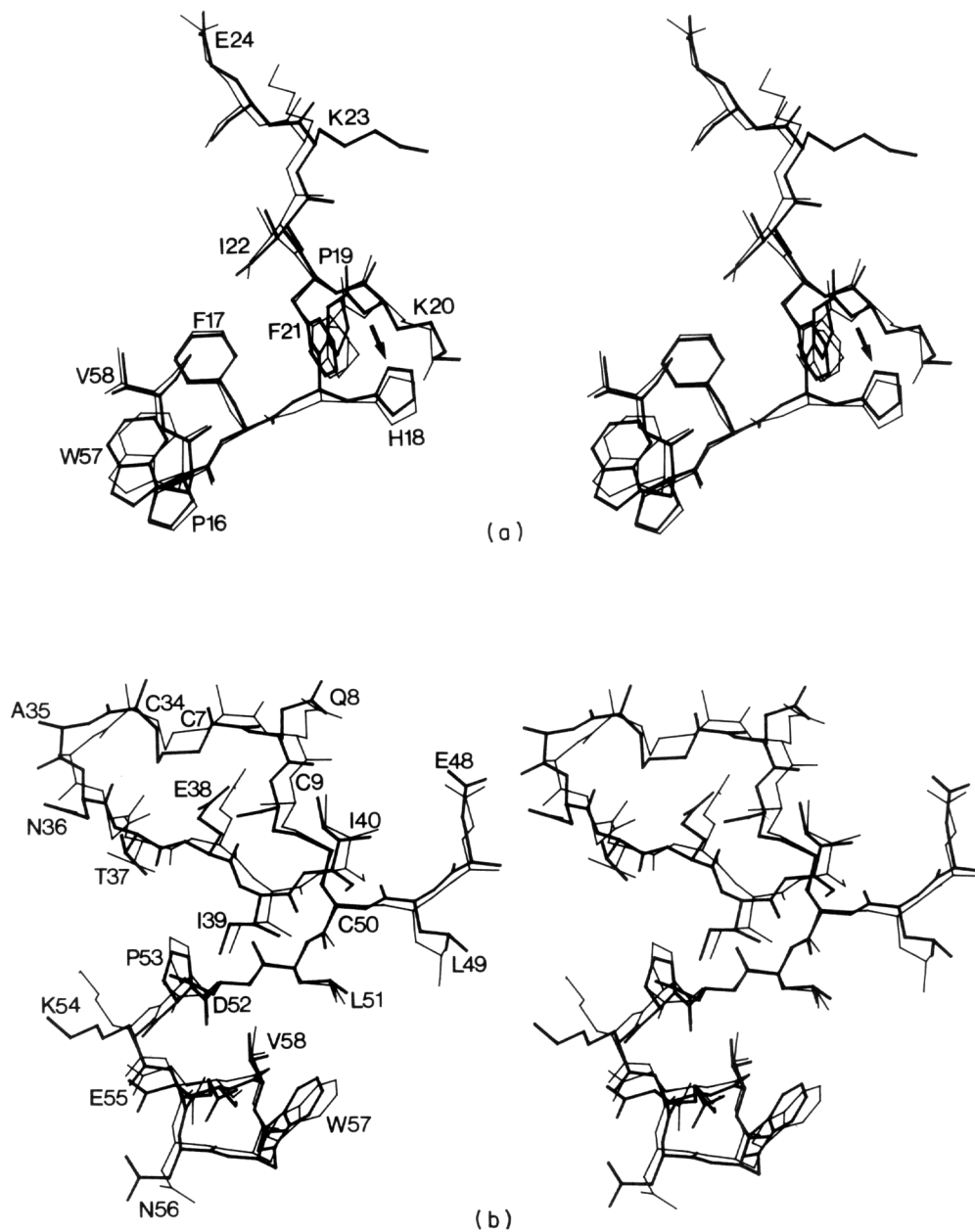


Figure 3. Best-fit superposition showing all atoms (excluding protons) of selected regions of the restrained minimized mean n.m.r. (thick lines) and X-ray (thin lines) structures of IL-8. Residues 16 to 24 and 57 to 58 are shown in (a), while residues 7 to 9, 34 to 40 and 48 to 58 are shown in (b). Note that the conformations of the 2 disulfide bridges between Cys7 and 34 and Cys9 and 50, seen in (b), are the same in the n.m.r. and X-ray structures. The arrow in (a) indicates the hydrogen bond from the backbone amide of Lys20 (donor) to the N³¹ atom of the imidazole ring of His18 (acceptor).

orientation of the two subunits. The average overall ϕ and ψ angular r.m.s. differences between the 30 SA structures and the X-ray structure are $16.1^\circ (\pm 13.3^\circ)$ and $17.8^\circ (\pm 13.3^\circ)$, respectively.

The atomic r.m.s. differences at the monomer level for some regions of the structure are larger than the errors in both the X-ray (about 0.2 to

0.3 Å) and n.m.r. co-ordinates. This is based on the criteria that, for these regions, either the atomic or ϕ , ψ angular r.m.s. differences between the 30 SA structures and the X-ray structure are greater by more than two standard deviations than the atomic r.m.s. differences between the 30 SA structures and the mean co-ordinate positions, or the average pair-

Figure 2. (a) and (b) Two views of best-fit superpositions of the backbone atoms of the monomer unit of the restrained minimized mean n.m.r. (thick lines) and X-ray (thin lines) structures of IL-8. (c) and (d) Two views of best-fit superpositions (to 1 monomer) of the backbone atoms of the restrained minimized mean n.m.r. (thick lines) and X-ray (thin lines) structures of IL-8. The difference in the angle between the 2 central β -strands (residues 23 to 29 and 23' to 29') and in the distance between the 2 helices is clearly seen in (c) and (d), respectively. Residues 4 to 5 are partially disordered in solution and therefore shown as dotted lines.

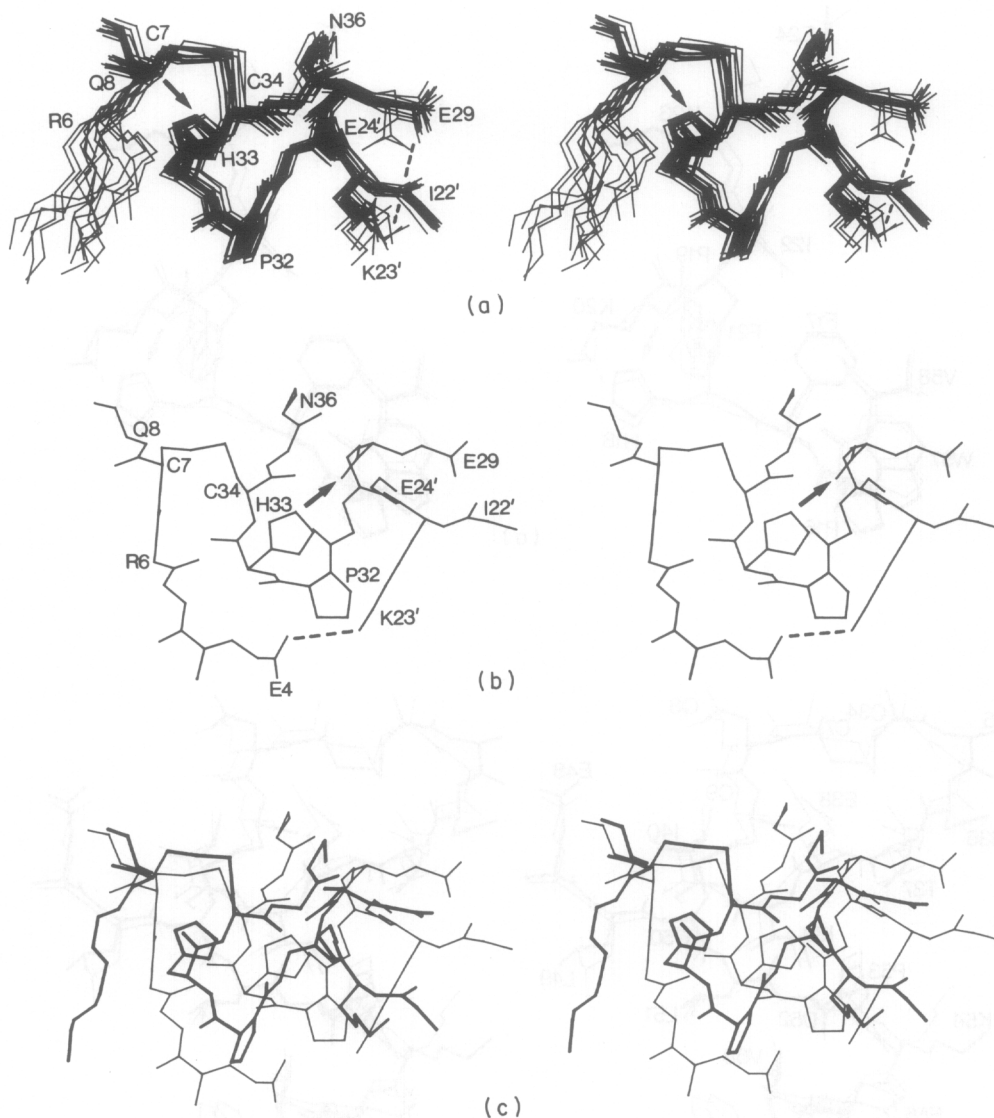


Figure 4. Comparison of the 31 to 36 loop and its associated interactions in the n.m.r. and X-ray structures of IL-8. (a) Superposition of 15 SA n.m.r. structures; (b) view of the X-ray structure in the same orientation; and (c) superposition of restrained minimized mean n.m.r. (thick lines) and X-ray (thin lines) structures. The backbone atoms of residues 4 to 8, 29 to 36 of one subunit and residues 22' to 24' of the other subunit are shown, together with the side-chains of Glu4 (X-ray structure only), Cys7, Glu29, Pro32, His33 and Cys34 of one subunit and Lys23' of the other subunit. The arrows indicate hydrogen bonds involving the imidazole ring of His33: in the n.m.r. structure the $N^{\epsilon 2}$ atom of His33 accepts a hydrogen bond from the backbone amide of Gln8, while in the X-ray structure the $N^{\epsilon 2}H$ atom of His33 donates a hydrogen bond to the backbone carbonyl group of Glu29. The broken lines indicate electrostatic interactions: in the case of the n.m.r. structure there is an electrostatic interaction between the side-chain carboxylate group of Glu29 of one subunit and the $N^{\epsilon}H_3^+$ group of Lys23' of the other, while in the X-ray structure the carboxylate group of Glu4 of one subunit is in close proximity with the $N^{\epsilon}H_3^+$ group of Lys23 of the other.

wise ϕ , ψ r.m.s. differences between the individual SA structures, respectively. For the backbone atoms notable differences are observed at the N terminus (residues 4 to 10), and at residues 14, 19, 27 to 37, 39 to 41, 44, 54, 61, 62 and 70 to 72, the largest involving the N terminus and the 31 to 36 loop. These differences, however, were not sufficient to prevent the successful application of molecular replacement to solve the X-ray structure using the n.m.r. structure as a starting model (Baldwin *et al.*, 1990), and the similarity between both structures is clearly apparent from the overall structural comparison shown in Figure 2(a) and (b).

There is good correspondence in the conformations of the internal side-chains and no differences in the χ_1 rotamer conformations are observed for these residues between the two sets of structures. This is well illustrated in Figure 3, which shows best-fit superpositions including side-chains for two selected regions of the protein. In particular, the conformations of the two disulfide bridges are the same in the n.m.r. and X-ray structures (Fig. 3(b)). Some differences, however, are seen in the case of surface-accessible side-chains. For ten residues (L5, R6, K20, K23, K26, N36, S44, Q59, E70 and N71), the χ_1 rotamer conformations differ in the n.m.r. and

X-ray structures. In the case of another eight residues (K11, K15, K42, E48, N56, R60, E63 and L66), the χ_1 angle has been placed in only a single rotamer population in the X-ray structure, whereas the $^3J_{\alpha\beta}$ coupling constants have values of 6 to 7 Hz, indicating that they are disordered in solution. It is easily possible that these differences at the surface of the protein may be attributable to crystal packing forces. In addition, further refinement of the X-ray structure may reveal the presence of multiple conformations for these side-chains.

Focussing on the main regions of difference between the n.m.r. and X-ray structures, we observe that residues 4 to 6 are ill defined in the n.m.r. structure but well defined in the crystal structure (Baldwin *et al.*, 1990). From the X-ray structure one would predict one NOE between the $C^\beta H$ protons of Glu4 and His33, three NOEs between side-chain protons of Leu5 and Gln8 and one NOE between the backbone NH of Leu5 and the $C^\beta H$ proton of His33, on the basis of interproton distances ≤ 3.5 Å for these interactions, which are clearly not observed in solution. Further examination of the X-ray structure reveals the presence of an electrostatic interaction between the carboxylate of Glu4 of one subunit and the $N^{\delta}H_3^+$ group of Lys23' of the other subunit (the 2 oppositely charged groups being separated by < 4.5 Å and potentially by ≤ 2.5 Å when the side-chain χ torsion angles of Glu4 are adjusted to their idealized values; Figs 1 and 4(b)). This electrostatic interaction fixes the conformation of the N-terminal residues in the X-ray structure. In the n.m.r. structure residues 4 to 6 are not well ordered, although it is apparent from Fig. 1 that the polypeptide chain at the N terminus runs in a different direction for the n.m.r. *versus* the X-ray structure, and the electrostatic interaction observed in the crystal structure is completely absent and replaced by an electrostatic interaction between the carboxylate of Glu29 of one subunit and the $N^{\delta}H_3^+$ group of Lys23' of the other subunit (Fig. 4(a)). The different electrostatic interactions involving Lys23 in the crystal and solution structures may be due to crystal packing forces, as well as to differences in the solution conditions used for the two studies (pH 5.2 and low ionic strength for the n.m.r. *versus* pH 8.5 and very high ionic strength for the crystallization). In this regard it should be noted that pH alone cannot be responsible for these differences, as no discontinuities in the pH dependence of the chemical shifts are observed over the pH range 2.6 to 8.5 (our unpublished results). Further, no changes in the n.m.r. spectrum could be observed as the salt concentration was increased up to 200 mM-NaCl. It is also worth recalling that the above finding is reminiscent of the situation in bovine pancreatic trypsin inhibitor, where large differences (greater than 4 Å and up to 8 Å) in the positions of the two C-terminal residues are apparent between crystal forms I and III on the one hand, and crystal form II and the solution structure on the other, and arise from the absence and presence, respectively, of a salt bridge between the

N-terminal amino group and the C-terminal carboxyl group (Wlodawer *et al.*, 1987a,b; Wagner *et al.*, 1987).

The second region of substantial difference between the n.m.r. and X-ray structures within the monomer unit relates to the location of the loop 31 to 36 (Figs 2 and 4). Given the high quality of both the X-ray and n.m.r. data, this divergence must reflect a genuine difference between the structures in solution and in the solid state. In both structures, this loop is covalently attached to the N-terminal strand through the disulfide bridge between Cys7 and Cys34, and the difference between the two structures has its most pronounced manifestation in the presence of different interactions involving the imidazole ring of His33 (Fig. 4). In solution, the $N^{\epsilon 2}$ atom of His33 accepts a hydrogen bond from the backbone NH group of Gln8, accounting for both the observed low pK_a of His33 (pK_a 4.9 with a titration shift of ~ 1 p.p.m. for the $C^{\epsilon 1}H$ proton and classical Henderson-Hasselbalch titration behavior) and the extreme downfield chemical shift of the NH of Gln8, which resonates at 11.94 p.p.m. at pH 5.2. In contrast, in the crystal structure the $N^{\epsilon 2}H$ atom of His33 donates a hydrogen bond to the backbone carbonyl group of Glu29. This, together with the absence of any neighboring positive charge, would predict a $pK \geq 6.5$ for His33. An analogous situation has been observed in hemoglobin and is associated with the R (deoxy) to T (oxy) transition responsible for the Bohr effect: in particular, the imidazole side-chain of the C-terminal His HC3(146) β in the T state forms a salt bridge with an aspartate FG1(94) of the same β -chain and has a high pK_a , while in the R state His HC3(146) β accepts a hydrogen bond from its own NH and has a low pK_a (Perutz *et al.*, 1987).

In the light of the different interaction involving His33 in the n.m.r. and X-ray structures, it is interesting to note that the second histidine residue in IL-8 at position 18 is also involved in hydrogen bonding, and in both the n.m.r. and X-ray structures the imidazole $N^{\delta 1}$ atom accepts a hydrogen bond from the backbone NH of Lys20 (Fig. 3(a)). The pK_a of this histidine is also extremely low ($pK_a = 3.7$, with a titration shift of ~ 1 p.p.m. for the $C^{\epsilon 1}H$ proton and classical titration behavior) and the NH resonance of Lys20 (at 11.53 p.p.m. at pH 5.2) displays a similarly large extreme downfield chemical shift to that of Gln8 (Clare *et al.*, 1989, 1990). In addition, the chemical shifts of the NH resonances of both Gln8 and Lys20 show essentially no pH dependence above pH 5, but shift rapidly upfield as the pH is decreased below 5, such that at pH 3.4 they both have shifts of 9.75 p.p.m. This demonstrates that both these amide protons are involved in strong interactions that are only disrupted at pH values below 5, indicative of hydrogen bonding with the corresponding imidazole rings at pH values above the pK_a of the histidine residues.

The origin for the different conformations of the 31 to 36 loop in the two structures may be attri-

buted to two factors. First, in the crystal structure Pro32 is tightly packed in a hydrophobic pocket formed by Tyr13, Phe17, Phe21 and Leu43 of an adjacent molecule in the crystal lattice, and the position of the carbonyl group of Pro32 is further determined by an electrostatic interaction with the side-chain of Arg47 of a neighboring molecule. Second, the electrostatic interaction between Glu4 of one subunit and Lys23' of the other in the crystal structure prevents the loop, and in particular His33, from coming into hydrogen bonding range of the NH of Gln8. In this light, it is worth bearing in mind that local differences in loop positions of both similar and larger magnitude have been reported for several crystallographically determined structures: for example, between different molecules in the unit cell for the crystal structures of adenylate kinase (Sachsenheimer & Schulz, 1977), bovine chymotrypsinogen A (Wang *et al.*, 1985), aspartate carbamoyltransferase (Krause *et al.*, 1987) and oxidized *Escherichia coli* thioredoxin (Katti *et al.*, 1990).

In addition to the differences at the level of the monomer, there is also a significant difference between the quaternary structures of IL-8 in solution and in the crystal that relates to the relative orientation of the two subunits (Fig. 2(c) and (d)). Thus, when subunit A of both structures is superimposed, the backbone atomic r.m.s. shift between subunit B of the two structures is ~ 4.4 Å. Differences of similar magnitude in the orientation of one subunit relative to another have been observed in two different crystal forms of the Bence-Jones protein Loc (Schiffer *et al.*, 1989), and in the case of the catabolite activator (or cyclic AMP receptor) protein different relative orientations of the N- and C-terminal domains are observed in two chemically identical subunits within the dimer (Weber & Steitz, 1987).

The main result of the difference in quaternary structure is that the separation and angle between the long axes of the two helices is 11.1 Å and 164° in the crystal structure *versus* 14.8 Å and 172° in the solution structure. In this regard it has to be emphasized that the relative orientation of the two subunits in the solution structure is determined only by the experimental n.m.r. restraints as the non-bonded term of the target function is represented solely by a quartic van der Waals repulsion term, and no Lennard-Jones, electrostatic or hydrogen bonding terms are used in the n.m.r. structure calculations (Nilges *et al.*, 1988; Clore *et al.*, 1990). The X-ray structure also predicts an additional 30 interproton distances less than 4 Å (corresponding to 15 NOEs due to the symmetrical nature of the dimer), of which ten are between 3.0 and 3.5 Å, and eight are ≤ 3 Å between the two subunits, which are clearly not observed in solution as evidenced by the absence of any NOEs corresponding to these contacts (Table 2). Additionally, the X-ray structure exhibits 52 interproton distance violations between 0.5 and 2 Å with respect to the experimental n.m.r. restraints. Thus, when the crystal structure is subjected to simulated annealing

Table 2
Dimer contacts predicted to give rise to NOEs by the X-ray structure of IL-8 but not observed experimentally in solution

Subunit 1	Subunit 2	Interproton distance (Å)	
		X-ray	n.m.r. (SA) _r
Lys23(C ^β H)	Glu29'(C ^β H)	3.5	5.2
Val27(NH)	Leu25'(C ^γ H)	3.9	5.1
Val27(C ^β H)	Leu66'(C ^{β1} H)	3.9	6.8
Val27(C ^{γ1} H)	Leu66'(C ^α H)	3.9	4.7
Val27(C ^{γ1} H)	Leu66'(C ^{β2} H)	3.4	4.3
Val27(C ^{γ1} H)	Leu66'(C ^{β2} H)	2.9	4.3
Val27(C ^{γ1} H)	Ala69'(C ^β H)	3.7	4.2
Ile28(C ^α H)	Glu24'(C ^γ H)	3.2	4.1
Glu29(C ^γ H)	Ala69'(C ^β H)	3.2	4.1
Leu66(C ^{β1} H)	Val62'(C ^{γ1} H)	2.9	7.2
Leu66(C ^{β2} H)	Val62'(C ^{γ1} H)	3.3	6.0
Glu70(C ^α H)	Pro53'(C ^β H)	2.2	5.2
Glu70(C ^α H)	Pro53'(C ^β H)	3.9	5.4
Glu70(C ^β H)	Pro53'(C ^β H)	3.8	6.4
Glu70(C ^γ H)	Gln59(C ^γ H)	3.0	7.2

against a target function comprising the interproton distances, it is converted back into a structure that falls well within the envelope of the individual simulated annealing n.m.r. structures. Interestingly, the interhelical separation in the AB dimer of the crystal structure of the related platelet factor 4 (PF4) is the same as that in the solution structure of IL-8 (St Charles *et al.*, 1989). The origin for the different width of the cleft between the helices is seen in Figure 2(c) and arises from the different angle between the long axes of the two central strands of the β -sheet at the dimer interface formed by residues 23 to 29 of the two subunits. Whereas in the solution structure of IL-8, as well as in the crystal structure of PF4, these two strands are at an angle of $\sim 168^\circ$, commonly found in regular β -sheets, in the IL-8 crystal structure the central sheet is virtually flat, with an angle of $\sim 179^\circ$. In contrast, the angle between strands 1 (residues 23 to 30) and 2 (residues 35 to 43), and strands 2 and 3 (residues 46 to 53) are essentially the same in the solution and X-ray structures with values typical for a classical β -sheet (140° to 170°). Because the helices run almost orthogonal to the strands, the actual angle being around 60° , a reduction in the angle between axes of the central strands brings the helices closer together and decreases the angle between their long axes. Thus, the difference in quaternary structure arises from a rigid body rotation of the two subunits about the C_2 axis of symmetry that preserves the symmetrical relationship of the two subunits. Inspection of the two structures suggests that the difference in the twist of the central β -strands is intimately related to the two differences at the monomer level described above acting in synergy. Thus, the relative orientation of the two strands reflects the different interactions at both the N- and C-terminal ends of the strands, in particular the electrostatic interaction between

Lys23' of one subunit and the carboxylate group of either Glu4 or Glu29 of the other, and the hydrogen bonding interaction of His33 with either the backbone carbonyl group of Glu29 or amide of Gln8, respectively.

On the basis of the similarity of the general architecture of IL-8 to that of the $\alpha 1/\alpha 2$ domains of the human class I histocompatibility antigen HLA-A2 (Bjorkman *et al.*, 1987), we previously suggested that the two helices and the cleft between them form the binding site for the cellular receptor (Clore *et al.*, 1990). This hypothesis is supported by a number of experiments involving alterations in the residues at the surface of the helices that reduce the binding of IL-8 to its receptor by a factor of 10 to 100 (K. Matsushima, E. Appella, G.M.C. and A.M.G., unpublished results). This leads us to propose a further extension of this model in which the differences in quaternary structure in the solution and crystal states, "open" with a large interhelical cleft *versus* "closed" with a small interhelical cleft, respectively, may be of functional significance. This model suggests a possible avenue for the rational design of IL-8 inhibitors as it predicts that any molecule that would inhibit the quaternary conformational changes from taking place would also inhibit IL-8 from eliciting its usual biological response. Such an inhibitor need be directed to bind not only to the helices and the cleft between them, but also to parts of the N terminus (Glu4 to Cys9) and 31 to 36 loop, both of which form a single contiguous surface projecting from the edge of the β -sheet into solution. The possible relevance of these residues with regard to the mechanism of action of IL-8 is suggested by sequence comparisons of IL-8, human GRO and murine MIP-2, all of which bind to the same receptor on neutrophils and elicit an identical response, namely neutrophil chemotaxis (Matsushima & Oppenheim, 1989; Leonard *et al.*, 1990). In particular, the stretch of residues from Glu4 to Cys9 and Gly31 to Cys34 are conserved in all three proteins, and the residue at position 23, either a Lys (IL-8) or a Gln (GRO and MIP-2), can potentially take part in an electrostatic interaction with Glu4 of the other subunit. PF4 from various sources (bovine, human and rat), on the other hand, displays only weak neutrophil chemotaxis activity (Leonard *et al.*, 1990). Apart from the effect of a number of substitutions at the surface of the two helices that result in two charge alterations (Glu63 \rightarrow Lys or Gln and Lys67 \rightarrow Asp, Ala or Ser), it may well be the case that PF4 cannot undergo the conformational transition between the "open" and "closed" states as Glu4 is substituted by Asp and Lys23 by Ser (bovine PF4) or Thr (human and rat PF4). Both these side-chains are too short to permit any significant electrostatic interaction between them. Hence, the quaternary structure of PF4 remains similar to that of the "open" form of IL-8 represented by the n.m.r. structure. This interpretation is further supported by the observation that, just as in the solution structure of IL-8, the residues on the N-terminal side of the first cysteine residue

are disordered in the crystal structure of bovine PF4 (St Charles *et al.*, 1989).

Despite the attractive features of the above model, it should be borne in mind that at this time there is no direct evidence that the different quaternary structures of IL-8, "open" *versus* "closed", seen in solution and in the crystal state, are of functional significance. The difference between the solution and crystal state may arise purely from crystal lattice forces favoring one conformation over another. Nevertheless, the observation of these different states indicates that IL-8 has the potential to undergo conformational transitions, and it seems likely that this property may be relevant to the mode of binding to its cell surface receptor and to the mechanism whereby it elicits a biological response.

We thank Drs A. Wlodawer, E. Baldwin and J. Moutl for many useful discussions. This work was supported by the AIDS Directed Anti-Viral Program of the Office of the Director of the National Institutes of Health.

References

- Baldwin, E. T., Weber, I. T., St Charles, R., Xuan, J.-C., Appella, E., Yamada, M., Matsushima, K., Edwards, B. F. P., Clore, G. M., Gronenborn, A. M. & Wlodawer, A. (1990). Crystal Structure of Interleukin-8: Symbiosis of NMR and Crystallography. *Proc. Nat. Acad. Sci., U.S.A.* in the press.
- Bjorkman, P. J., Saper, M. A., Samraoui, B., Bennett, W. S., Strominger, J. L. & Wiley, D. C. (1987). Structure of the Human Class I Histocompatibility Antigen HLA-A2. *Nature (London)*, **329**, 506-512.
- Clore, G. M., Appella, E., Yamada, M., Matsushima, K. & Gronenborn, A. M. (1989). Determination of the Secondary Structure of Interleukin-8 by Nuclear Magnetic Resonance Spectroscopy. *J. Biol. Chem.* **264**, 18907-18911.
- Clore, G. M., Appella, E., Yamada, E., Matsushima, K. & Gronenborn, A. M. (1990). Three-dimensional Structure of Interleukin-8 in Solution. *Biochemistry*, **29**, 1689-1696.
- Katti, S. K., LeMaster, D. M. & Eklund, H. (1990). Crystal Structure of Thioredoxin from *Escherichia coli* at 1.68 Å Resolution. *J. Mol. Biol.* **212**, 167-184.
- Krause, K. L., Volz, K. W. & Lipscomb, W. N. (1987). 2.5 Å Structure of Aspartate Carbamoyltransferase Complexed with the Bisubstrate Analog *N*-(Phosphoacetyl)-L-aspartate. *J. Mol. Biol.* **193**, 527-553.
- Leonard, E. J. & Yoshimura, T. (1990). Neutrophil Attractant/Activation Protein-1 {NAP-1 (IL-8)}. *Am. J. Resp. Cell Mol. Biol.*, in the press.
- Leonard, E. J., Yoshimura, T., Walz, A., Baggiolini, M., Walz, D. A., Goetzl, E. J. & Castor, C. W. (1990). Chemotactic Activity and Receptor Binding of Neutrophil Attractant/Activation Protein-1 (NAP-1) and Structurally Related Host Defense Cytokines: Interaction of NAP-2 with NAP-1 Receptor. *J. Leuk. Biol.*, in the press.
- Matsushima, K. & Oppenheim, J. J. (1989). Interleukin-8 and MCAF: Novel Inflammatory Cytokines Inducible by IL-1 and TNF. *Cytokine*, **1**, 2-13.
- Nilges, M., Clore, G. M. & Gronenborn, A. M. (1988). Determination of Three-dimensional Structures of

- Proteins from Interproton Distance Data by Hybrid Distance Geometry-dynamical Simulated Annealing Calculations. *FEBS Letters*, **229**, 317-324.
- Perutz, M. F., Fermi, G., Luisi, B., Shaanan, B. & Liddington, R. C. (1987). Stereochemistry of Cooperative Effects in Haemoglobin. *Acct. Chem. Res.* **20**, 309-321.
- Sachsenheimer, W. & Schulz, G. E. (1977). Two Conformations of Crystalline Adenylate Cyclase. *J. Mol. Biol.* **114**, 23-36.
- Schiffer, M., Ainsworth, C., Xu, Z.-B., Carperos, W., Olsen, K., Solomon, A., Stevens, F. V. & Chang, C.-H. (1989). Structure of a Second Crystal Form of Bence-Jones Protein Loc: Strikingly Different Domain Associations in Two Crystal Forms of a Single Protein. *Biochemistry*, **28**, 4066-4072.
- St Charles, R., Walz, D. A. & Edwards, B. F. P. (1989). The Three-dimensional Structure of Bovine Platelet Factor 4 at 3.0 Å Resolution. *J. Biol. Chem.* **264**, 2092-2099.
- Wagner, G., Braun, W., Havel, T. F., Schaumann, T., Go, N. & Wüthrich, K. (1987). Protein Structures in Solution by Nuclear Magnetic Resonance and Distance Geometry: The Polypeptide Fold of the Basic Pancreatic Trypsin Inhibitor Determined Using Two Different Algorithms, DISGEO and DISMAN. *J. Mol. Biol.* **196**, 611-639.
- Wang, D., Bode, W. & Huber, R. (1985). Bovine Chymotrypsinogen A: X-ray Crystal Structure Analysis and Refinement of a New Crystal Form at 1.8 Å Resolution. *J. Mol. Biol.* **185**, 595-624.
- Weber, I. T. & Steitz, T. A. (1987). Structure of a Complex of Catabolite Gene Activator Protein and Cyclic AMP Refined at 2.5 Å Resolution. *J. Mol. Biol.* **198**, 311-326.
- Wlodawer, A., Deisenhofer, J. & Huber, R. (1987a). Comparison of Two Highly Refined Structures of Bovine Pancreatic Trypsin Inhibitor. *J. Mol. Biol.* **193**, 145-156.
- Wlodawer, A., Nachman, J., Gilliland, G. L., Gallagher, W. & Woodward, C. (1987b). Structure of Form III Crystals of Bovine Pancreatic Trypsin Inhibitor. *J. Mol. Biol.* **198**, 469-480.
- Yoshimura, T., Matsushima, K., Tanaka, S., Robinson, E. A., Appella, E., Oppenheim, J. J. & Leonard, E. (1987). Purification of a Human Monocyte-derived Neutrophil Chemotactic Factor that Shares Sequence Homology with Other Host Defense Cytokines. *Proc. Nat. Acad. Sci., U.S.A.* **84**, 9233-9237.

Edited by P. E. Wright